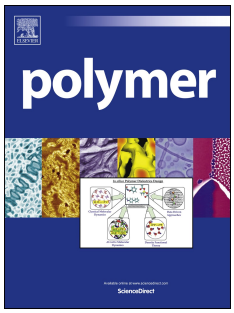

Integration of 3D printing with acoustic-assisted assembly of nanomaterials for tunable strain sensors

Yun Li, Deana Yuan, Mingyuan Sun, Kathryn Feddish, Liang Zhao, Bo Li

PII: S0032-3861(24)00633-5

DOI: https://doi.org/10.1016/j.polymer.2024.127297

Reference: JPOL 127297

To appear in: *Polymer*

Received Date: 26 March 2024

Revised Date: 13 June 2024

Accepted Date: 15 June 2024

Please cite this article as: Li Y, Yuan D, Sun M, Feddish K, Zhao L, Li B, Integration of 3D printing with acoustic-assisted assembly of nanomaterials for tunable strain sensors, *Polymer*, https://doi.org/10.1016/j.polymer.2024.127297.

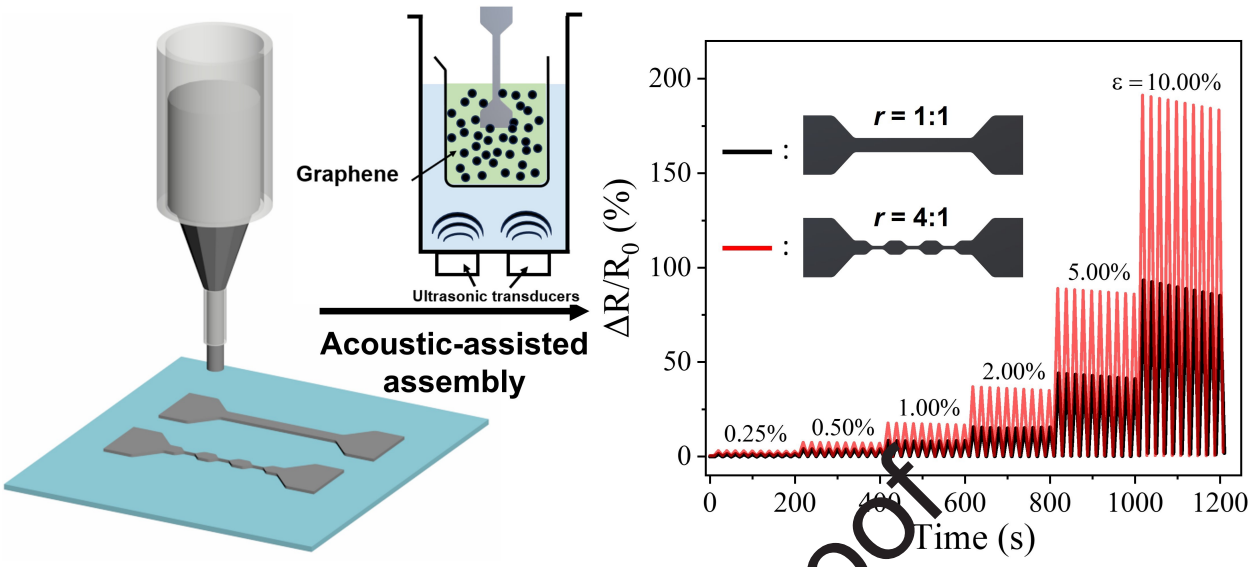

Material extrusion

Strain sensors performance

Integration of 3D printing with acoustic-assisted assembly of nanomaterials for tunable strain sensors

Yun Li[a,b], Deana Yuan[b,c], Mingyuan Sun[a,b], Kathryn Feddish[b,d], Liang Zhao[a,b], Bo Li[a,b,*]

[a] Department of Mechanical Engineering, Villanova University, Villanova, PA 19085, USA.

[b] Hybrid Nano-Architectures and Advanced Manufacturing Laboratory, Villanova University, Villanova, PA 19085, USA

[c] Department of Comprehensive Science, Villanova University, Villanova, PA 19085, USA

[d] Department of Chemical Engineering, Villanova University, Villanova, PA 19085, USA

[*] Corresponding author. Email address: bo.li@villanova.edu (B. Li)

Abstract

This study reports a novel methodology for the development of tunable strain sensors by leveraging 3D printing for structural designs and nanomaterial assembly for functional layer coating. We utilized material extrusion (MEX) to print sensor substrates using composite ink of polydimethylsiloxane (PDMS) and silica nanoparticles. MEX allows us to create a non-uniform strain distribution of the sensor substrate by designing alternating wide and thin strips with different mechanical properties along the stretching direction. Then, we assembled nanometer-thick graphene flakes on the surface of the substrate using an acoustic-assisted dip-coating method to construct strain sensors. The graphene network on the narrow strips will experience large deformation leading to significantly increased resistance. By fixing the width of wide strips and tailoring the width ratio of the wide strip over narrow strips (*r*), the gauge factor can be controlled from 8.53 (r = 1:1) to 33.15 (r = 16:1). Also, by printing the narrow strips with softer PDMS, the sensitivity of the sensor can be further increased. The research pioneers the integration of 3D printing and nanomaterial assembly for strain sensors. More importantly, it paves the way for the generic design of flexible electronics and other hybrid systems of polymer and nanomaterials.

Keywords: Strain Sensor, Material Extrusion, Graphene, Polydimethylsiloxane, Dip-Coating

Introduction

Flexible strain sensors that can sense motion, sound, touch, and pulse found important applications in health care and automation[1-5]. This technology has gained significant attention due to its commercial use in smart electronic devices and wearable devices, especially real-time health monitoring systems[6, 7]. With proper biochemical properties, these sensors can be used to monitor food, glucose, sweat, etc.[8-10]. Other applications include human motion detection, soft robotics, electronic skin, and medical diagnosis[6, 7, 11, 12]. Compared to conventional sensors, which are rigid, bulky, and usually cannot achieve real-time monitoring, flexible sensors can be manipulated into different geometries, thus allowing them to reach multiple fields. The flexibility allows for higher sensitivity, mechanical flexibility, and a faster response time[13]. In the case of resistance sensors, the mechanical deformation can break down its conductive network, leading to increased resistance[14-18].

While most polymers used for the matrix of the sensor substrate are insulating, conductive nanomaterials (e.g., graphene and carbon nanotube) are mixed into the polymer to create a conductive composite[19-23]. A significant amount of conductive nanomaterials are needed to achieve a 3D continuous conductive network in a polymer matrix. The minimum loading to form the continuous conductive network is called the percolation threshold. When high conductivity is required, the loading of conductive nanomaterial should be further increased. However, conductive nanomaterials are expensive and significantly elevate the price of the sensors. In the field of nanocomposites, how to increase the filling efficiency and lower the loading of expensive nanomaterials have been studied extensively[23-26]. One interesting concept is creating a segregated structure where nanomaterials are mixed with polymer particles and through controlling the temperature of a hot-plate compression process, nanomaterials are sandwiched between deformed polymer particles, rather than diffusing into the polymer particles[27, 28]. The nanomaterials form a highly conductive network only at the interfaces, resulting in a significantly reduced percolation threshold.

3D printing technologies, such as material extrusion (MEX) and fused deposition modeling (FDM), have demonstrated the capability to print conductive polymer composite into flexible sensors with different geometries[29-31]. Unfortunately, 3D printing faces the same challenge of extensive nanomaterial usage. The concept of placing nanomaterials only on the interface/surface of a printed structure rather than into it inspired this study where the assembly technology of

nanomaterial is integrated with the MEX process to design strain sensors with controlled performance. We will use an acoustic-assisted dip-coating method, a water-based assembly process, to achieve uniform assembly of hard-to-wet graphene onto hydrophobic polydimethylsiloxane (PDMS) surfaces[32-34]. MEX offers strong capabilities in controlling ink printability and tailoring the mechanical properties and the structures of the part[35-39]. The combination of the two enables low-cost and green manufacturing of 3D printable sensors with controlled sensitivity.

2. Experimental

2.1 Materials

PDMSs: The SYLGARD™ 184 (purchased from Dow Corning Corp, USA), the DOWSIL™ SE 1700 (provided by Dow Corning Corp, Japan). Spherical SiO_2 nanoparticles (vendor-labeled 800 nm, US Research Nanomaterials Inc., USA). Graphene: ~5 μm in lateral dimension and 6–8 nm in thickness, with a surface area of 120 to 150 m^2/g (purchased from XGSciences, USA)

2.2 Preparation of nanoparticles-polymer composite inks

Nanoparticles-polymer composite inks were prepared by first blending two silicone elastomers: a shear-thinning PDMS material SE 1700 and a low-viscosity PDMS material Sylgard 184 which was used to dilute SE 1700 for desired rheological properties. Both SE 1700 and Sylgard 184 base materials were first mixed with their curing agents in a 10:1 (base: curing agent) ratio by weight before blending. SE 1700 and Sylgard 184 were mixed in a weight ratio of 7:3. Then, SiO_2 nanoparticles were added into the PDMSs and thoroughly stirred to obtain nanoparticles-polymer composite inks. The weight portion of PDMS was fixed as 100 and the SiO_2 nanoparticles increased from 0 to 20 portions. Final inks were loaded into a 5 mL syringe (Allevi, USA) at room temperature and centrifuged at 3000 rpm for 15 mins to remove any air bubbles.

2.3 Material extrusion of the composite ink

A luck-lock plastic tip (330 μm) was attached to the syringe and then loaded into the printing head. The inks were printed using a 3D printer (Allevi 3 Bioprinter, Allevi Inc., USA). A compressed air pneumatic system was used to pressurize the syringe and control the ink's flow rate. The printing parameters were fixed: 6 mm/s for printing speed (i.e., nozzle moving speed), and 60 psi (4.17×10^5 Pa) for pressure. After printing, the samples were put into an oven at 80 °C for 2 hours to complete the curing.

2.4 Acoustic-assisted dip-coating assembly

A 50 mg/mL graphene solution was prepared and ultrasonicated in a sonication bath (40 kHz, 60 W) for one hour. Dip-coating was performed using a custom-built dip-coater at 1.524 m/min. The PDMS substrate was fixed on the holder and experienced cyclic dip coating process. The sonication was on during the whole assembly process. The PDMS samples were kept submerged in the graphene solution during the coating process. The dip-coating time varied from 1 to 15 minutes in the graphene solution to investigate the effect of coating duration. After dip-coating, the graphene-coated PDMS samples were dried with compressed nitrogen gas to remove excess solution, ensuring uniform graphene coatings.

2.5 Characterizations

Scanning Electron Microscopy (SEM) images were acquired using Hitachi S-4800. The electrical properties of the coatings were assessed using a Keithley 2400 source meter. Resistance measurements were carried out by employing the two-probe method to ensure accurate determination of the electrical conductivity of the graphene layer. In detail, nanoparticles-polymer composite ink was prepared and spin-coated on glass slides (25 mm x 25 mm x 1 mm) at a speed of 8000 rpm for 2 minutes. The coated slides were then cured in an oven at 80°C for 2 hours. Following this initial preparation, the samples went through a dip-coating process identical to that described in section 2.4. To measure the thickness of the coated graphene layer, atomic force microscopy (AFM) images were taken by an atomic force microscope (Park System NX10) using a scan rate of 0.5 Hz. To establish electrical contacts, silver paste was 3D printed onto the surface of the graphene coating forming six straight lines, each 25 mm in length and 0.4 mm in width with a central spacing of 5 mm between them. These lines were left to dry for 24 hours. For resistance measurement, a Keithley 2400 source meter's probes were connected to the ends of two adjacent silver lines, separated by 5 mm, to measure the resistance across the graphene coating. The mechanical properties of the 3D printed dog-bone shaped samples with different nanoparticles loadings were tested using a Psylotech μTS. The sensing performance of the graphene-coated strain sensors was evaluated using a Psylothch μTS test system in conjunction with a Keithley 2400 source meter. Samples were fixed to the tensile tester system with a gap of 25 mm between two clamps. To maintain a consistent testing duration across different strains, stretching speeds of 6.25, 12.5, 25, 50, 125, and 250 μm/s were applied for strains of 0.25%, 0.5%, 1%, 2%, 5%, and 10%, respectively. Each strain level was repeated 10 times to assess the repeatability of the sensor's

response. The change in resistance during the application of strain was recorded in real-time, providing insights into the sensor's sensitivity under various strains.

3. Results and discussion

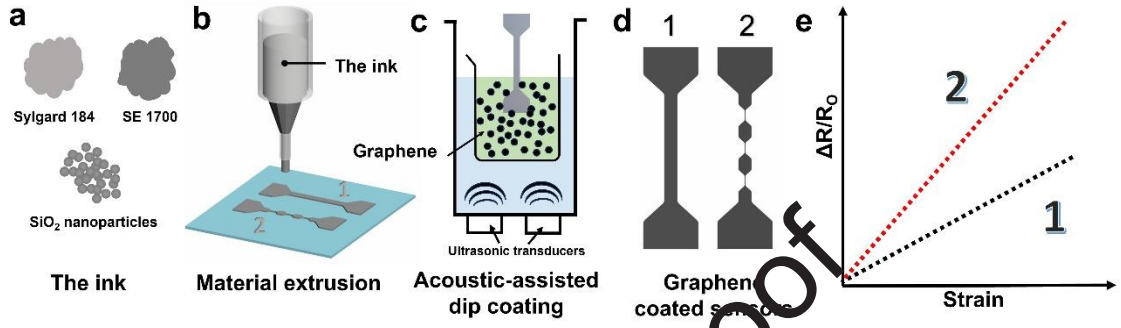

Fig. 1. Schematic overview of the experimental workflow for fabricating graphene-coated PDMS strain sensors with enhanced sensitivity. (a) The printable ink design for material extrusion. (b) Material extrusion process with different pattern designs. (c) The sonication-assisted dip-coating method. (d) Various pattern designs after dip-coating. (e) Different sensing performances between designs under various strains.

This research aims to combine the enriched design capability of 3D printing with nanomaterial assembly technology for the development of sensors (Fig. 1). We will utilize strain sensors as the demonstration system. The MEX method is an extremely inclusive 3D printing method that can integrate different materials —such as polymers, solvents, and nanoparticles — in one extrusion-based printing process (Fig. 1a). By tailoring the composition of the ink, the printability of inks (or gels) and the mechanical properties of the resultant parts can be controlled. More importantly, MEX can print complex mechanical structures to further design the mechanical characteristics of the parts (Fig. 1b). For example, if we compare two dog-bone sensor designs: sample 1 with a fixed cross-section and sample 2 with alternating wide and narrow strips, we could create locally highly deformed regions (i.e., narrow strips) even though a small deformation is applied to the sensor. If we assemble a conductive nanomaterials network on both sensors, the mechanical characteristics can be translated into integrated electrical properties (Fig. 1c-1e). If we consider narrow and wide strips as resistors on a series circuit, the narrow strips amplify the signal as the deformation of the narrow strips can be much larger than the overall strain of the sample. However,

the sensor with a fixed cross-section does not have such an amplification mechanism; therefore, it is expected to have lower sensitivity (Fig. 1e).

We have developed an acoustic-assisted dip-coating method that can directly assemble hydrophobic nanomaterials, such as graphene, on 3D printed PDMS substrates[32, 40]. The graphene powder was dispersed in water using an ultrasound bath (40 kHz at 60W) and then the printed samples were submerged in the graphene solution using a customized dip coater (Fig. 1c and 1d). The resultant strain sensors are expected to achieve different sensitivities by tailoring the mechanical and geometric design in MEX such as the width ratio (r) of the wide to narrow strips of the printed parts and the mechanical properties of the wide and narrow strips.

3.1 Optimization of Silica Nanoparticle Concentration for Enhanced Printability and Mechanical Performance

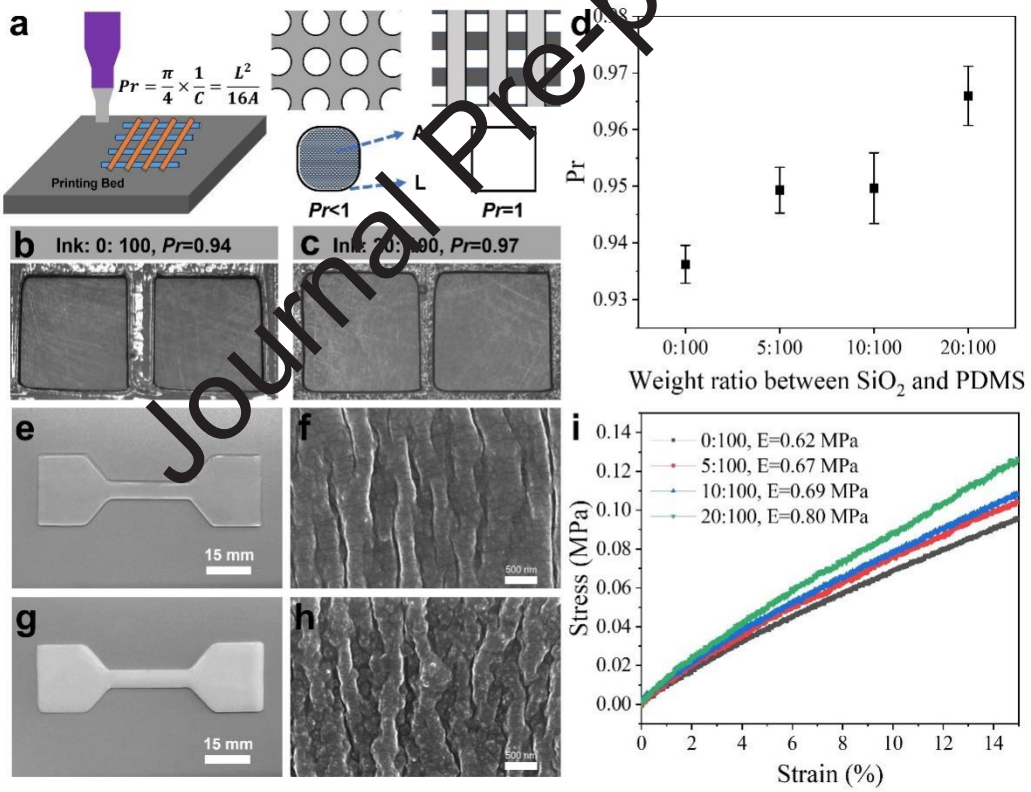

Fig. 2. (a) A simplified diagram illustrating the DLPA method and the cases where *Pr* is less than 1 and equal to 1. (b, c) Representative top-view images of a crisscrossed printed layer using different ratios and corresponding *Pr*. (d) The relationship between silica nanoparticle concentration and *Pr*. (e) Photograph of dog-bone shaped printed sample with 0:100 ratio. (f) SEM image of printed sample with 0:100 SiO_2/PDMS weight ratio. (g) Photograph of dog-bone shaped

printed sample with 20:100 weight ratio. (h) SEM image of printed sample with 20:100 ratio. (i) The engineering strain-stress curve of printed samples with different compositions.

To print sensors with high shape stability and controlled mechanical properties, a comprehensive analysis was conducted to determine the ideal ratio of SiO_2 nanoparticles to PDMSs. Dual Layer Printability Analysis (DLPA) technique serves as a quantitative measure of an ink's printability. DLPA assesses the printability (*Pr*) of an ink by observing the merging behavior of crisscrossed printed layers (Fig. 2a). The procedure entails printing two perpendicular layers under uniform printing speed and pressure. We first define the circularity (*C*) in order to define printability (*Pr*)[41] as follows:

$$C = \frac{4\pi A}{L^2} \tag{1}$$

where *L* and *A* are the perimeter and area of the pores, respectively. The shape of the enclosed area is closest to a circle when *C* is equal to 1. Since the highest circularity for a square shape is equal to π/4, the *Pr* of an ink based on a printed square shape is defined as follows:

$$Pr = \frac{\pi}{4} \times \frac{1}{C} = \frac{L^2}{16A} \tag{2}$$

Ideally, if the layers maintain their integrity without merging, perfect square patterns can be achieved (*Pr*=1). Conversely, if the two layers merge well, the squares will degrade into circles and the *Pr* value will be less than 1(Fig. 2a). We fixed the weight portion of PDMS as 100 and increased SiO_2 nanoparticles portion from 0 to 20. Fig. 2b and 2c illustrate the top view image of the crisscrossed area for 0:100 ratio and 20:100 ratio formulas. The experimental findings illuminated by DLPA, which are shown in Fig. 2d, reveal a gradual improvement of the *Pr* value with an increase in SiO_2/PDMS ratio, with the value reaching around 0.97 when the ratio was 20:100. The inks showcased a promising trend of enhanced printability, manifesting in the superior structural integrity of the printed patterns. The comparison of samples with 0:100 and 20:100 ratios, both visually and under SEM (Fig. 2f and Fig 2h), highlighted the impacts of nanoparticle addition on surface texture and mechanical properties. Notably, the incorporation of nanoparticles resulted in a rougher surface texture and a marked increase in Young's modulus, from 0.62 MPa at 0:100 to 0.80 MPa at 20:100 (Fig. 2i), signifying an improvement in mechanical strength of the printed parts. Further increasing the loading of nanoparticles leads to printing instability (e.g., broken lines

due to the discontinued extrusion), therefore, the 20:100 nanoparticle to PDMS ratio was identified as the optimal composition for the following sensor design.

3.2 Correlation Between Dip Coating Duration, Graphene Layer Thickness, and Conductivity Enhancement

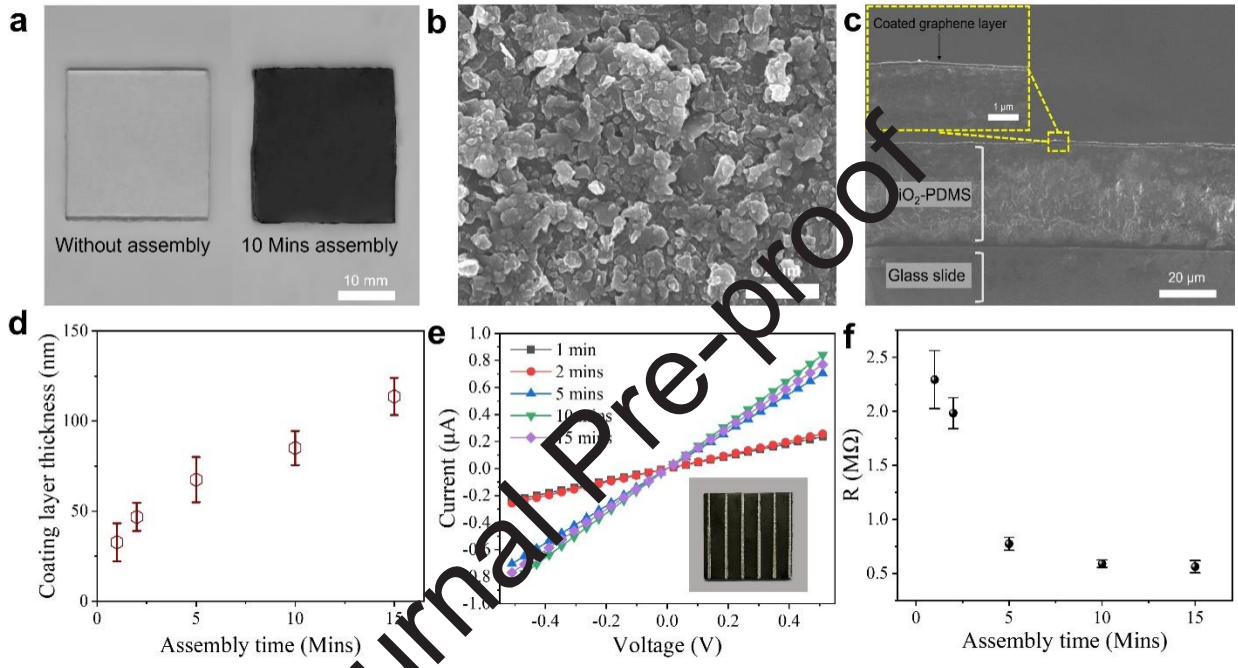

Fig.3. (a) Comparative images of a PDMS substrate coated on a glass slide before and after a 10-minute dip coating process. (b) Top view SEM image of the glass slide surface after 10 minutes of dip coating. (c) Cross section view SEM image of the glass slide surface after 10 minutes of dip coating. (d) Correlation between dip coating time and graphene layer thickness through AFM scanning analysis. (e) Representative I-V curves for samples subjected to different dip coating times, with an inset showing the 3D-printed silver electrodes for electrical measurements. (f) Correlation between dip coating time and graphene layer's electrical resistance measured from I-V tests.

To ensure high sensitivity, a continuous but sensitive conductive network is desirable. On the one hand, a continuous network ensures a conductive network across the electrodes. On the other hand, the number of conductive paths in the conductive network should not be too large such that the broken paths upon deformation lead to a large resistance change and high sensitivity. Here,

we utilized the acoustic-assisted dip-coating process to assemble graphene directly onto the surface of PDMS and studied how assembly time affects the assembly thickness and resistance. To examine the thickness of the assembled graphene layer, we spun coat SiO_2/PDMS ink (with 20:100 weight ratio) on a glass slide to ensure molecular-level flatness. Fig. 3a compares the original PDMS substrate before and after a 10 min graphene assembly. The morphology of the graphene network was further examined using SEM as shown in Fig. 3b and 3c. The images suggest that most graphene flakes are aligned parallel to the PDMS surface with a few standing flakes. The thickness of the resultant graphene assembly was characterized using AFM and the thickness increased from 32 nm at 1 min to 114 nm at 15 min (Fig. 3d). A representative AFM scanning image and corresponding line profile is provided in Supporting information (Fig.S1). The electrical measurement was performed by printing arrays of silver electrodes on the graphene surface and measuring I-V curves across the neighboring electrodes (inset image of Fig. 3e). The results suggest a percolation behavior where a continuous conductive network starts to form. Correspondingly, the resistances of the graphene assembly significantly decreased from 2 MΩ at 2 min to 780 kΩ at 5 min assembly. After the percolation, further increasing the assembly time leads to a slow decrease in the resistance. When reaching 10 min assembling, the resistivity of the graphene network reached 0.25 Ω·m (Fig. 3e-3f). We chose to use the 10 min as the assembly time for the strain sensors fabrication. The network of 5 min assembly can be premature while the 15 min assembly can be too stable. 10 min assembly leverages the integrity of the conductive network as well as its sensitivity against external deformation.

3.3 Sensing performance of strain sensors with different structural designs

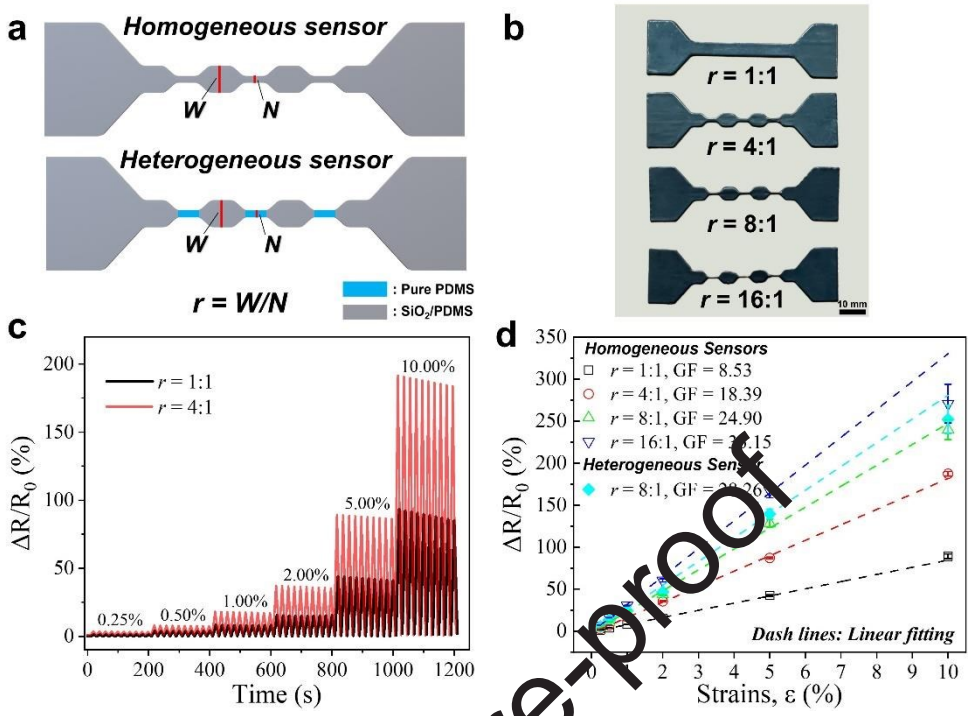

Fig. 4. (a) Schematic of the dog-bone-shaped sensor designs with different combinations of wide and narrow strips. The width ratio (r) of wide and narrow strips varies from 1:1 to 16:1. The overall length of the sensor and the width of the wide strip are fixed. (b) Photographic images of the graphene-coated sensors corresponding to the varying design ratios. (c) Representative relative resistance changes-time curves under cyclic strains ranging from 0.25 % to 10 % (r = 1:1 and 4:1). The resistance change is recorded over ten cycles at each strain level. Due to the overlapping of the curves, the relative resistance changes-time curves of r =8:1 and 16:1 are presented in supporting information (Fig.S2). (d) Peak resistance changes vs strains for all four sensor designs.

To fabricate the strain sensors, we have combined the MEX's capability to achieve PDMS substrate with controllable printability and geometries and acoustic-assisted dip coating process to coat conductive graphene layers on the surface of PDMS. As shown in Fig. 4a, we have designed dog-bone-shaped sensor designs with changing width ratios (r = W/N) of the wide (W) and narrow (N) strips. W is fixed as 4.8 mm and N was reduced from 4.8 mm to 0.3 mm. Therefore, r varies from 1:1 to 16:1. We can create homogeneous sensors with the same ink (ink weight ratio of SiO_2 to PDMS = 20:100) and heterogeneous sensors with harder wide strips (ink weight ratio = 20:100) and softer narrow strips (ink weight ratio = 0:100). A representative image of the graphene-coated sensors is presented in Fig. 4b and the strain sensing characterizations are summarized in Fig. 4c

and 4d. For homogeneous sensors, under the same strain, the narrow strips as well as the graphene network on them will deform much more than the wide strips. Therefore, with a smaller *N* (higher *r*), the graphene network shows better sensitivity as demonstrated in Fig. 4c. We have summarized data for all four homogeneous sensors in Fig. 4d, and gauge factors ($GF = (R-R_0)/R_0/\varepsilon$) of the sensors increased from 8.53 (*r* = 1:1) to 33.15 (*r* = 16:1).

We also fixed *r* = 8:1 and created a heterogeneous sensor by printing the narrow strips using the ink without SiO_2. The Young's modules of the pure PDMS (for narrow strips) and SiO_2/PDMS (for wide strips) were 0.62 MPa and 0.80 MPa, respectively. The heterogeneous sensor with softer narrow strips shows further improved sensitivity (GF = 28.26) in comparison with the homogenous sensor (GF = 24.90) with the same width ratio (*r* = 8:1). Under the same overall strain, the softer PDMS narrow strips in the heterogenous sensor undergo more deformation than the SiO_2/PDMS narrow strips in the homogenous sensor. This greater deformation leads to a more pronounced change in resistance (ΔR) of heterogenous sensors compared to that of the homogeneous sensors. The combined mechanical and structural control demonstrates a large design space for sensing applications. Such design space can be further enlarged with improved printing resolution (e.g., reduced strip width) and new ink materials with different mechanical properties.

4. Conclusion

In summary, we have successfully demonstrated the integration of 3D printing and nanomaterial assembly for strain sensor design. Unlike traditional strain sensors based on nanomaterial-filled conductive polymer composites, our method demonstrates a large design space for structures and mechanical properties of the sensor, lower usage of expensive conductive nanomaterials, and tunable sensitivity. More importantly, our method can be generalized to the design of flexible electronics and other hybrid systems and benefit the field of health care, sensing and actuation, and automation.

Acknowledgement:

Y.L., L.Z., and B.L. were supported in part by the National Science Foundation (Grant No. 2221102 and 2003077), PA Manufacturing Fellows Initiative, Sport & Performance Engineering Seed Grant of College of Engineering, Villanova University, Villanova University Startup Fund, and University Summer Grant of Villanova University. Y.L, and D.Y. were supported by the Small Research Grant; K.F. was supported by Clare Boothe Luce Engineering Scholars Program; and

D.Y. and K.F. was supported by the Villanova Match Research Program for First Year Students of Villanova University.

References

[1] T.Q. Trung, N.E. Lee, Flexible and stretchable physical sensor integrated platforms for wearable human-activity monitoringand personal healthcare, Advanced materials 28(22) (2016) 4338-4372.
[2] R.B. Mishra, N. El-Atab, A.M. Hussain, M.M. Hussain, Recent progress on flexible capacitive pressure sensors: From design and materials to applications, Advanced materials technologies 6(4) (2021) 2001023.
[3] Y. Huang, X. Fan, S.C. Chen, N. Zhao, Emerging technologies of flexible pressure sensors: materials, modeling, devices, and manufacturing, Advanced functional materials 29(12) (2019) 1808509.
[4] H. Liu, Q. Li, S. Zhang, R. Yin, X. Liu, Y. He, K. Dai, C. Shan, J. Guo, C. Liu, Electrically conductive polymer composites for smart flexible strain sensors: a critical review, Journal of Materials Chemistry C 6(45) (2018) 12121-12141.
[5] M.A.U. Khalid, S.H. Chang, Flexible strain sensors for wearable applications fabricated using novel functional nanocomposites: A review, Composite Structures 284 (2022) 115214.
[6] B. Zazoum, K.M. Batoo, M.A.A. Khan, Recent advances in flexible sensors and their applications, Sensors 22(12) (2022) 4653.
[7] C. Ma, B. Zhu, Z. Qian, L. Ren, H. Yuan, Y. Meng, 3D-printing of conductive inks based flexible tactile sensor for monitoring of temperature, strain and pressure, Journal of Manufacturing Processes 87 (2023) 1-10.
[8] D. Song, X. Chen, M. Wang, Z. Wu, X. Xiao, 3D-printed flexible sensors for food monitoring, Chemical Engineering Journal (2023) 146011.
[9] H. Liu, H. Zhang, W. Han, H. Lin, R. Li, J. Zhu, W. Huang, 3D printed flexible strain sensors: from printing to devices and signals, Advanced Materials 33(8) (2021) 2004782.
[10] W. Yang, Y. Qin, Z. Wang, T. Yu, Y. Ge, Recent advances in the development of flexible sensors: mechanisms, materials, performance optimization, and applications, Journal of Electronic Materials 51(12) (2022) 6735-6769.
[11] S. Ma, J. Tang, T. Yan, Z. Pan, Performance of flexible strain sensors with different transition mechanisms: a review, IEEE Sensors Journal 22(8) (2022) 7475-7498.
[12] Y. Zheng, R. Yin, Y. Zhao, H. Liu, D. Zhang, X. Shi, B. Zhang, C. Liu, C. Shen, Conductive MXene/cotton fabric based pressure sensor with both high sensitivity and wide sensing range for human motion detection and E-skin, Chemical Engineering Journal 420 (2021) 127720.
[13] F. Han, M. Li, H. Ye, G. Zhang, Materials, electrical performance, mechanisms, applications, and manufacturing approaches for flexible strain sensors, Nanomaterials 11(5) (2021) 1220.
[14] D. Liu, C. Huyan, Z. Wang, Z. Guo, X. Zhang, H. Torun, D. Mulvihill, B.B. Xu, F. Chen, Conductive polymer based hydrogels and their application in wearable sensors: a review, Materials Horizons 10(8) (2023) 2800-2823.
[15] M. Qu, Z. Xie, S. Liu, J. Zhang, S. Peng, Z. Li, C. Lin, F. Nilsson, Electric resistance of elastic strain sensors—fundamental mechanisms and experimental validation, Nanomaterials 13(12) (2023) 1813.
[16] M.J. Cordill, O. Glushko, B. Putz, Electro-mechanical testing of conductive materials used in flexible electronics, Frontiers in Materials 3 (2016) 11.
[17] J. Lee, S. Kim, J. Lee, D. Yang, B.C. Park, S. Ryu, I. Park, A stretchable strain sensor based on a metal nanoparticle thin film for human motion detection, Nanoscale 6(20) (2014) 11932-11939.

[18] Y. Qin, Q. Peng, Y. Ding, Z. Lin, C. Wang, Y. Li, F. Xu, J. Li, Y. Yuan, X. He, Lightweight, superelastic, and mechanically flexible graphene/polyimide nanocomposite foam for strain sensor application, ACS nano 9(9) (2015) 8933-8941.
[19] K. Huang, S. Dong, J. Yang, J. Yan, Y. Xue, X. You, J. Hu, L. Gao, X. Zhang, Y. Ding, Three-dimensional printing of a tunable graphene-based elastomer for strain sensors with ultrahigh sensitivity, Carbon 143 (2019) 63-72.
[20] D. Xiang, X. Zhang, Z. Han, Z. Zhang, Z. Zhou, E. Harkin-Jones, J. Zhang, X. Luo, P. Wang, C. Zhao, 3D printed high-performance flexible strain sensors based on carbon nanotube and graphene nanoplatelet filled polymer composites, Journal of Materials Science 55 (2020) 15769-15786.
[21] X. Chen, X. Zhang, D. Xiang, Y. Wu, C. Zhao, H. Li, Z. Li, P. Wang, Y. Li, 3D printed high-performance spider web-like flexible strain sensors with directional strain recognition based on conductive polymer composites, Materials Letters 306 (2022) 130935.
[22] W.-B. Zhu, S.-S. Xue, H. Zhang, Y.-Y. Wang, P. Huang, Z.-H. Tang, Y.-Q. Li, S.-Y. Fu, Direct ink writing of a graphene/CNT/silicone composite strain sensor with a near-zero temperature coefficient of resistance, Journal of Materials Chemistry C 10(21) (2022) 8226-8233.
[23] J. Britton, K. Krukiewicz, M. Chandran, J. Fernandez, A. Poudel, J.-R. Sarasua, U. FitzGerald, M.J. Biggs, A flexible strain-responsive sensor fabricated from a biocompatible electronic ink via an additive-manufacturing process, Materials & Design 206 (2021) 109700.
[24] S. Khan, L. Lorenzelli, Recent advances on conductive nanocomposites in printed and flexible electronics, Smart Materials and Structures 26(8) (2017) 083001.
[25] C. Zhan, G. Yu, Y. Lu, L. Wang, E. Wujcik, S. Wei, Conductive polymer nanocomposites: a critical review of modern advanced devices, Journal of Materials Chemistry C 5(7) (2017) 1569-1585.
[26] C. Park, M.S. Kim, H.H. Kim, S.-H. Sunwoo, D.J. Jung, M.K. Choi, D.-H. Kim, Stretchable conductive nanocomposites and their applications in wearable devices, Applied Physics Reviews 9(2) (2022).
[27] H. Pang, L. Xu, D.-X. Yan, Z.-M. Li, Conductive polymer composites with segregated structures, Progress in Polymer Science 39(11) (2014) 1908-1933.
[28] D.X. Yan, H. Pang, B. Li, R. Vajtai, L. Xu, P.G. Ren, J.H. Wang, Z.M. Li, Structured reduced graphene oxide/polymer composites for ultra-efficient electromagnetic interference shielding, Advanced Functional Materials 25(4) (2015) 559-566.
[29] J.T. Muth, D.M. Vogt, R.L. Truby, Y. Mengüç, D.B. Kolesky, R.J. Wood, J.A. Lewis, Embedded 3D printing of strain sensors within highly stretchable elastomers, Advanced materials 26(36) (2014) 6307-6312.
[30] Z. Wang, Q. Zhang, Y. Yue, J. Xu, W. Xu, X. Sun, Y. Chen, J. Jiang, Y. Liu, 3D printed graphene/polydimethylsiloxane composite for stretchable strain sensor with tunable sensitivity, Nanotechnology 30(34) (2019) 345501.
[31] S. Agarwala, G.L. Goh, T.-S. Dinh Le, J. An, Z.K. Peh, W.Y. Yeong, Y.-J. Kim, Wearable bandage-based strain sensor for home healthcare: Combining 3D aerosol jet printing and laser sintering, ACS sensors 4(1) (2018) 218-226.
[32] D. Zhou, M. Han, B. Sidnawi, Q. Wu, Y. Gogotsi, B. Li, Ultrafast assembly and healing of nanomaterial networks on polymer substrates for flexible hybrid electronics, Applied Materials Today 22 (2021) 100956.

[33] L. Zhao, B. Sidnawi, J. Fan, R. Chen, T. Scully, S. Dietrich, W. Gao, Q. Wu, B. Li, Wafer-Scale Full-Coverage Self-Limiting Assembly of Particles on Flexible Substrates, ACS Applied Materials & Interfaces 14(40) (2022) 46095-46102.
[34] L. Zhu, J. Lang, D. Zhou, Q. Wu, B. Li, Fluid-Assisted Sorted Assembly of Graphene on Polymer, Langmuir 36(20) (2020) 5608-5617.
[35] Y. Li, B. Li, Direct ink writing 3D printing of polydimethylsiloxane-based soft and composite materials: a mini review, Oxford Open Materials Science 2(1) (2022) itac008.
[36] M. Saadi, A. Maguire, N.T. Pottackal, M.S.H. Thakur, M.M. Ikram, A.J. Hart, P.M. Ajayan, M.M. Rahman, Direct ink writing: a 3D printing technology for diverse materials, Advanced Materials 34(28) (2022) 2108855.
[37] D. Mondal, T.L. Willett, Mechanical properties of nanocomposite biomaterials improved by extrusion during direct ink writing, Journal of the Mechanical Behavior of Biomedical Materials 104 (2020) 103653.
[38] L. Li, Q. Lin, M. Tang, A.J. Duncan, C. Ke, Advanced polymer designs for direct-ink-write 3D printing, Chemistry–A European Journal 25(46) (2019) 10768-10781.
[39] H. Feng, S. Wang, Y. Cui, Y. Xiang, X. Liu, X. Sun, W. Zhang, P. Tu, Effect of 3D printing process parameters on the mechanical properties of silica/polyethyleneimine composites using direct-ink writing, Polymer Composites 44(11) (2023) 7687-7700.
[40] D. Zhou, J. Lang, N. Yoo, R.R. Unocic, Q. Wu, B. Li, Fluid-guided CVD growth for large-scale monolayer two-dimensional materials, ACS applied materials & interfaces 12(23) (2020) 26342-26349.
[41] L. Ouyang, R. Yao, Y. Zhao, W. Sun, Effect of bioink properties on printability and cell viability for 3D bioplotting of embryonic stem cells, Biofabrication 8(3) (2016) 035020.

1. 3D printing creates tunable strain sensors with variable structural designs.
2. Gauge factor controllability ranges from 8.53 to 33.15 by adjusting strip width ratios.
3. Nanomaterial assembly enhanced by acoustic-assisted graphene coating.
4. Reduces nanomaterial usage, significantly increases sensor sensitivity.

Declaration of interests

☒ The authors declare that they have no known competing financial interests or personal relationships that could have appeared to influence the work reported in this paper.

☐ The authors declare the following financial interests/personal relationships which may be considered as potential competing interests: